*Research in Health & Medical Sciences* *Review Article*

*2024 October; 3(4)*

# Efficiency of photocatalytic processes in the removal of the antibiotic ciprofloxacin from aqueous environments: A systematic review

**Hossein Farash Khayalo*[1], Morteza Bahlgerdi[1], Ali Habibi[1]**

[1] Student research committee, School of public health, Iran University of Medical Sciences, Tehran, Iran

***Corresponding Author Email: hosseinfarash@gmail.com**
**Received: 2026/1; Revised: 2026/4; Accepted: 2026/4**

## Abstract

The widespread presence of the antibiotic ciprofloxacin (CIP) in aquatic environments poses severe ecological and public health risks due to its recalcitrant nature. Advanced oxidation processes, specifically semiconductor-based photocatalysis, have emerged as highly promising strategies for highly efficient CIP removal and mitigation of antimicrobial resistance.

This systematic review evaluates the efficiency of photocatalytic systems in removing CIP from aqueous environments. Following a comprehensive literature search across Scopus, Web of Science, Embase, and PubMed databases for studies published up to September 30, 69 peer-reviewed articles were selected and synthesized for in-depth analysis of operational parameters and degradation mechanisms.

The temporal distribution of the included literature demonstrates a rapid increase in research interest, particularly peaking between 2021 and 2024. Key operational variables governing degradation include optimal catalyst dosages of 0.1–1.0 g/L and reaction times of 60–120 minutes. Recent advancements highlight a shift towards visible-light and solar-driven photocatalysis using advanced Z-scheme and S-scheme heterojunctions. These systems frequently achieve >90% CIP removal, generally following pseudo-first-order kinetics. Mechanistically, reactive oxygen species drive the cleavage of quinolone and piperazine rings, yielding lower-toxicity transformation products. However, discrepancies between rapid parent compound removal and actual total mineralization remain prevalent.

While photocatalytic degradation of CIP is highly effective at the laboratory scale, reliance on synthetic wastewater and powder catalysts in batch slurry reactors hinders industrial scale-up. Future research must prioritize immobilized catalyst systems, continuous-flow reactors, real wastewater matrices, and standardized energy efficiency (EEo) reporting to bridge the gap toward real-world applications.

**Keywords:** Ciprofloxacin, Photocatalysis, Advanced oxidation processes, Heterojunction, Wastewater treatment, Systematic review.

## Introduction

The uncontrolled dissemination of pharmaceutical compounds in aquatic environments has become a growing global concern (1, 2). Among these pollutants, antibiotics particularly fluoroquinolones such as ciprofloxacin (CIP) are recognized as emerging contaminants due to their persistence, high stability, and resistance to conventional wastewater treatment processes (3-5). The widespread consumption of CIP in human and veterinary medicine has resulted in its frequent detection in surface waters, groundwater, and even drinking water, at concentrations ranging from nanograms to milligrams per liter (3, 6). The incomplete biodegradability and stable quinolone structure of CIP hinder its natural decomposition, facilitating its accumulation in ecosystems and promoting the evolution of antibiotic-resistant bacteria (3). Conventional biological and physicochemical treatment methods including adsorption, chlorination, and ozonation often fail to mineralize such recalcitrant compounds and may produce harmful by-products (7). Consequently, advanced oxidation processes (AOPs), particularly semiconductor-based photocatalysis, have emerged as promising alternatives for the degradation of CIP in aqueous systems (8, 9). These processes rely on the generation of highly reactive oxygen species (ROS), including hydroxyl (•OH) and superoxide ($O_2^{\bullet-}$) radicals, upon photoexcitation of a semiconductor under UV or visible light (10, 11). The ROS oxidize organic molecules, converting them into non-toxic end products such as $CO_2$ and $H_2O$ (12, 13). Among various semiconductors, $TiO_2$ has been extensively studied for photocatalytic degradation due to its stability and strong oxidizing potential (14-16). However, its wide bandgap (~3.2 eV) limits activity to the UV region, which represents less than 5% of the solar spectrum, while the rapid recombination of electron-hole pairs further diminishes efficiency (17, 18). To overcome these limitations, doping and heterojunction engineering have been widely adopted to extend light absorption into the visible region and enhance charge separation (16, 19). For instance, $Nd_2O_3/TiO_2$ nanocomposites exhibited up to eightfold higher photocatalytic activity compared to bare $TiO_2$, achieving complete CIP degradation within 150 minutes under visible light (20). Beyond $TiO_2$ systems, perovskite-based materials such as La-doped $NaTaO_3$ (LNTO) have shown excellent photocatalytic performance owing to their tunable electronic structure and chemical stability. Coupling LNTO with narrow bandgap oxides such as $\alpha$-$Fe_2O_3$ and $Bi_2O_3$ efficiently reduced the bandgap energy from 4.4 to ~2.3 eV and significantly improved charge carrier separation, enabling full degradation of CIP within 90–120 minutes under visible irradiation (21, 22). These perovskite systems demonstrated strong recyclability and structural stability, confirming their potential for sustainable water treatment applications. In addition, green-synthesized photocatalysts have gained increasing interest as environmentally friendly alternatives to conventional synthesis routes. For instance, $Co_3O_4$ quantum dots synthesized using tomato seed extracts successfully degraded CIP under UV light, offering a low-cost and biogenic pathway to produce efficient catalysts (23). Similarly, ZnO-functionalized fly ash composites have been proposed as eco-compatible materials combining industrial waste utilization with effective photocatalytic performance for antibiotic removal (24). Such green and waste-derived materials align with circular economy principles and reduce secondary pollution risks.

Recently, two-dimensional (2D) heterostructures have emerged as advanced platforms for visible-light-driven photocatalysis. Bi-doped NiAl-LDH/g-$C_3N_4$ composites, for example, displayed 86% CIP removal efficiency within 180 minutes under visible light due to improved charge mobility and interfacial contact between 2D layers (25). Likewise, RGO-bridged $CuFe_2O_4$@$Ag_2S$ S-scheme heterojunctions achieved complete CIP degradation under simulated sunlight, demonstrating excellent mineralization capacity (85% COD reduction) and reusability over six consecutive cycles (26).

Collectively, these advances highlight a strong research trend toward designing multifunctional, recyclable, and solar-active photocatalysts that combine material innovation, green synthesis, and mechanistic understanding for enhanced degradation of antibiotics.

Given the environmental significance and ongoing technological progress, a comprehensive assessment of photocatalytic efficiency, mechanisms, and influencing parameters across various systems is essential. Therefore, this systematic review aims to synthesize recent findings on ciprofloxacin degradation using diverse photocatalytic materials ranging from metal oxides and perovskites to hybrid and green-synthesized nanocomposites. The review consolidates insights into how structural design, dopants, light sources, and reaction conditions govern the degradation kinetics, stability, and reusability of photocatalysts, providing a holistic understanding of current advances and future prospects in antibiotic removal from aquatic environments.

## Materials and Methods

*Literature survey and search approach*

This systematic review was conducted in accordance with the Preferred Reporting Items for Systematic Reviews and Meta-Analyses (PRISMA) 2020 guidelines. Adherence to this framework ensures that the methodology is transparent, comprehensive, and reproducible. The subsequent sections provide a detailed account of the search strategy, the inclusion and exclusion criteria, the process of data extraction, and the analytical approach employed for the synthesis of the findings.

A systematic search covered four main electronic databases. These included Scopus, Web of Science, Embase and PubMed. The search was conducted with no lower date limit and included all available records up to September 30, 2025. To ensure comprehensiveness, articles formally published in 2025 that were available online as early access by the search date were also included. Search strategies were tailored for each database, and reference lists of eligible articles were manually screened for additional relevant studies.

An example of the search strategy we employed in Scopus is structured as follows:

(photocatal* OR "photo-catal*" OR "photocatal*" OR "photocatalytic" OR photocatalysis OR "heterogeneous photocatalysis" OR "visible light photocatal*" OR "visible-light photocatal*" OR TiO2 OR "titanium dioxide" OR ZnO OR g-C3N4 OR "graphitic carbon nitride" OR photocatalytic) AND (ciprofloxacin OR Cipro OR "ciprofloxacin hydrochloride") AND (water OR aqueous OR wastewater OR "wastewater" OR sewage OR "surface water" OR groundwater OR "drinking water" OR "environmental water" OR "aqueous solution") AND (remov* OR degrad* OR photo degrad* OR photolys* OR mineraliz* OR eliminat* OR "removal efficiency" OR "degradation rate" OR "rate constant" OR kinetics)

*Inclusion and Exclusion Criteria*

Eligibility criteria for all studies included: (1) experimental studies investigating photocatalytic processes applied for CIP removal from aqueous solution, (2) reports of quantitative results such as removal efficiencies, rate constants, or total organic carbon reductions, (3) reporting in English and (4) published in a peer-reviewed journal. Studies were excluded if they were: (1) a review, conference abstracts, or editorial, (2) an experiment unrelated to CIP or lacked any data/results on CIP, and (3) studies that presented no quantitative results.

*Study selection*

Two independent reviewers screened titles and abstracts for eligibility. The articles which were eligible for inclusion had their full text screened. A third reviewer mediated any conflicts. The selection process followed the 4 PRISMA phases: identification, screening, eligibility and inclusion. Of 4065 records initially retrieved, 69 studies met all inclusion criteria. A PRISMA flow diagram summarizing the selection process is presented in Figure 1.

*Data extraction*

A uniform data extraction instrument was employed to extract: (1) bibliographic information (author, year, country); (2) catalyst type and formulation; (3) experimental conditions (pH, initial CIP concentration, catalyst dosage, method and intensity of irradiation, reaction time); (4) performance outcomes (removal efficiency, rate constants); (5) catalyst stability and reusability; (6) mineralization efficiency (TOC removal); and (7) degradation pathway and toxicity investigations. Two reviewers independently extracted the data, with disagreements reconciled through discussion.

*Quality assessment*

To evaluate the methodological quality and risk of bias of the included studies, a customized appraisal was conducted. Criteria included the clarity of the experimental setup, inclusion of appropriate control groups (e.g., dark adsorption tests), reproducibility, and proper reporting of parameters. Studies were categorized to ensure that the data synthesized in this review originated from methodologically sound experiments with a low to moderate risk of bias.

*Data analysis*

Considering the diversity in experimental conditions, results were synthesized descriptively rather than combined into a meta-analysis. Trends in catalyst performance were evaluated in response to catalyst composition, operational conditions, and reported mechanisms of degradation. Wherever possible, ranges and medians were reported to summarize removal efficiencies and mineralization rates.

## Results and discussion

### Study selection process

The systematic literature search identified 4065 preliminary records in the target databases [Scopus: 1476, Web of Science: 1956, Embase: 305, and PubMed: 328]. After eliminating document duplication, 3129 distinct documents were screened. A total of 2070 articles that were not pertinent to the study were eliminated by evaluating their titles, leaving 1059 articles for abstract screening. Following this, 859 records were excluded because their abstracts did not meet the inclusion criteria, leaving 200 articles for the full-text review. After excluding 131 articles due to insufficient data, unrelated methodologies, or unrelated outcomes, 69 studies were included in the final synthesis. The extensive screening and selection procedures are shown in the PRISMA flow diagram (Figure 1).

### Light source publication and distribution

Figure 2 shows the distribution of the selected studies over time. As indicated, the number of publications is overall on an increasing trend with time, which shows the interest in more research in this direction. The peaks included 2024 [n=11], then 2022 [n=10], 2021 [n=10], and 2020 [n=10]. Several studies were also published in 2018 [n=7] and 2023 [n=6]. Few studies were published in 2019 [n=5], 2010 [n=3], 2025 [n=2], 2017 [n=2], 2016 [n=1], 2015 [n=1], and 2014 [n=1].

Figure 3 shows the distribution of light sources used in the studies. It can be seen that most of the research was conducted on visible light irradiation [37.7%], slightly more than UV irradiation [31.9%] and natural or simulated sunlight [30.4%]. This trend implies that research interest is moving toward the utilization of visible light and solar energy to achieve sustainable photocatalytic usage.

### Examples of photocatalysts in selected studies

Table 1 presents a comprehensive overview of the main characteristics of the studies reviewed, including the photocatalyst, light source, working conditions, and degradation rate. Various photocatalytic materials with a wide range of diversity have been generated and tested for CIP breakdown in aqueous solutions. These materials can be defined based on their composition and structural design. Photocatalysts based on metal oxides continue to be heavily researched because they are stable and possess strong oxidizing potential. An example would be $TiO_2$ nanotubes (NTAs) or $Nd_2O_3/TiO_2$ nanocomposites that

utilize dopants to extend light absorption into the visible region. Zinc oxide (ZnO) has also been used extensively, commonly in composite types like ZnO@FAU composites or functionalized with fly ash to combine industrial waste utilization with effective performance.

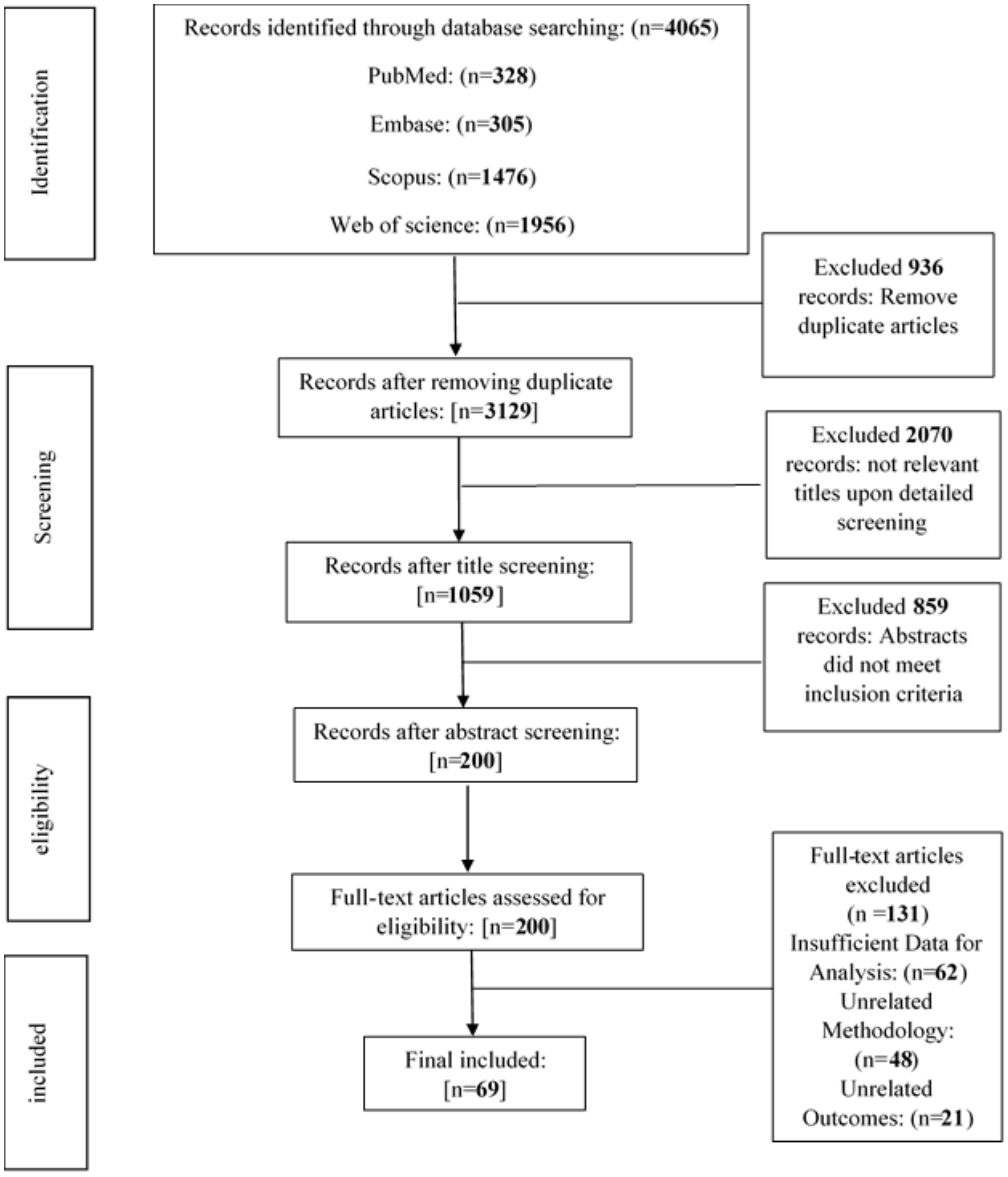


**Figure 1. PRISMA diagram for searching resources**

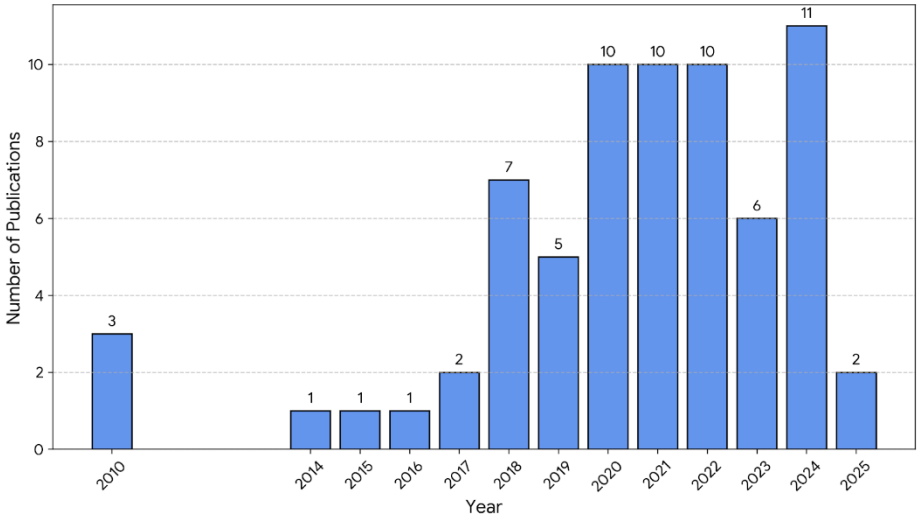


**Figure 2. Distribution of the selected studies on the photocatalytic degradation of ciprofloxacin over time (year of publication).**

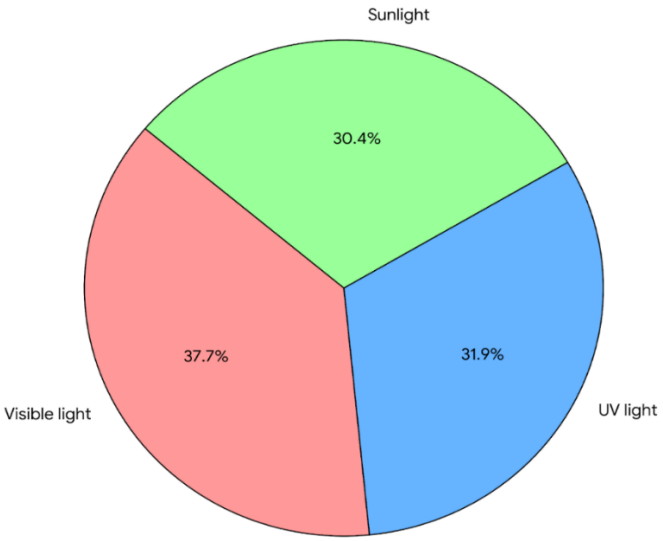


**Figure 3. Distribution of the various light sources (visible light, UV irradiation, and natural/simulated sunlight) utilized in the reviewed photocatalytic systems.**

Additionally, perovskite-based materials such as La-doped $NaTaO_3$ (LNTO) have been investigated, especially in heterojunction designs with narrow bandgap oxides like $\alpha$-$Fe_2O_3$, to enhance the gathering of visible light (22). Another important category includes Metal-Organic Frameworks (MOFs) and biochar composites, which offer high surface areas and sustainable synthesis routes. MOF-based and biochar composites, including PAN@ZnONPs/Bio-MOF and $Bi_2MoO_6$/Banana Peel Biochar, have been demonstrated to be

highly effective for CIP degradation (27). Finally, more complex 2D heterojunction systems, including S-scheme and Z-scheme designs, have been engineered so that the charge carriers are spatially separated. Examples include BiOX/GaMOF S-scheme heterojunctions and N-CQDs/$TiO_2$ S-scheme systems. A critical comparison between these materials reveals a trade-off between activity and stability (28, 29). While advanced heterojunctions generally offer superior visible-light harvesting compared to single metal oxides like bare $TiO_2$, industrial scale-up often requires mechanically robust and cost-effective synthesis routes.

**Operational and reaction conditions**

*Catalyst dosage [g/L]*

The concentration of the photocatalyst is an important factor that varies the quantity of active sites that can be utilized in the reaction and the penetration of light into the solution. The studies reviewed mention a broad spectrum of catalyst dosages ranging between 0.004 g/L and 4 g/L. In most cases, the degradation efficiency increases with increasing catalyst loading to an optimal level, after which light scattering and shielding effects occur owing to solution turbidity, and thus, the photoactivity is reduced. For example, Wei et al. employed a dosage of 0.5 g/L for $Bi_2MoO_6$/Banana Peel Biochar, and Tang et al. utilized 0.8 g/L for PAN@ZnONPs/Bio-MOF. In contrast, Huang et al. found success using lower amounts (0.2 g/L) for $TiO_2$@AMSF under UV light (30-32).

*PH*

- The pH of the solution has a significant effect on the photocatalyst's surface charge and the target molecule, changing the way the pollutant and the catalyst surface interact with each other. The best pH level depends on the material being used.
- **Acidic Conditions:** Numerous studies have indicated a preference for acidic environments. For example, Hayri-Senel et al. found that PS-$TiO_2$ composites worked effectively at pH=3 (33), while Alam et al. used a Mn/Co oxide nanocomposite optimally at pH=4 (34).
- **Neutral and Alkaline Conditions:** On the other hand, some systems work better in neutral or alkaline conditions. Mohamed et al. achieved efficient degradation at pH=8 utilizing a NiO@g-$C_3N_4$ nanocomposite (35). Similarly, El-Kemary et al. observed activity at pH=10 for ZnO nanoparticles (36). However, many studies indicated that a neutral pH (around 6-7) is highly effective, such as for the ZnO@FAU composite.
- The reported variation in optimal pH across studies highlights the critical role of electrostatic interactions.

*Time [min]*

The time it takes to get significant degradation through irradiation depends on how well the catalyst and light source work. Highly efficient catalysts, like the $TiO_2$ nanotubes (NTAs) that Abromaitis et al. (37), wrote about, broke down completely [100%] in 8 minutes of UV-C light. Similarly, Bouyarmane et al. (37),achieved 100% degradation in 15 minutes of UV light utilizing a TiHAp Nanocomposite. On the other hand, other systems needed more time. For instance, Huang et al. (38), used a 400-450-minute reaction time for $TiO_2$@AMSF, and Durán-Álvarez et al. (39), used a 300-minute reaction time for Z-scheme AgBr/Ag/$Bi_2WO_6$. Most studies, on the other hand, say that the best reaction time is between 60 and 120 minutes.

Figure 4 shows how degradation efficiencies are spread out over different reaction times. It shows that shorter times [like 8–30 minutes] can lead to high efficiencies with advanced catalysts, but most systems reach equilibrium in the 60–120-minute range.

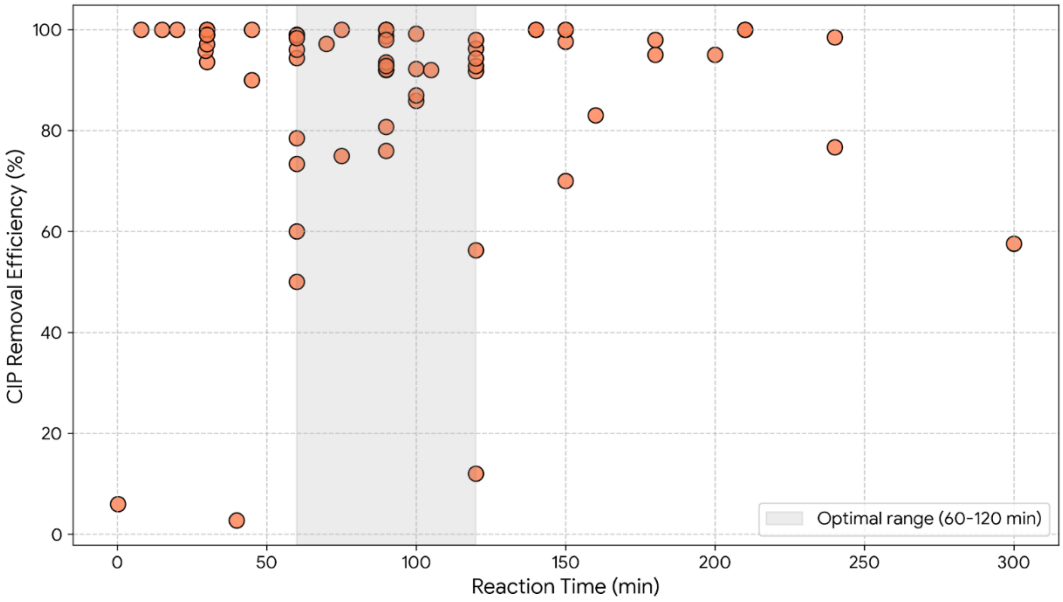


**Figure 4. Scatter plot illustrating the relationship between ciprofloxacin removal efficiency (%) and reaction time (min), highlighting the typical equilibrium range of 60–120 minutes.**

*Concentration [mg/L]*

The initial concentration of CIP was inversely related to degradation efficiency. Higher concentrations can saturate the active sites of the catalyst and reduce light penetration in the solution. The reviewed studies investigated a wide range of initial concentrations, from trace levels of 10 µM to higher loads of 50 mg/L. However, most research has focused on concentrations between 5 and 20 mg/L, reflecting typical experimental laboratory conditions. For instance, Chen et al. and Baldez et al. utilized 20 mg/L and 10 mg/L, respectively, achieving high removal rates (40). From a critical engineering perspective, a major limitation in the reviewed literature is the discrepancy between experimental concentrations and real-world conditions. While high concentrations facilitate easier kinetic monitoring in the lab, environmental CIP levels are typically found at concentrations ranging from nanograms to milligrams per liter. Future studies must evaluate photocatalytic performance at trace levels to accurately predict removal behavior in actual wastewater treatment plants.

*Degradation efficiency*

The reported photocatalysts generally exhibited high degradation efficiencies. Exceptionally high removal rates (100%) have been achieved using advanced composites such as Pt@$BiVO_4$-g-$C_3N_4$ and 3% CdO/La-$NaTaO_3$. Many other studies have reported efficiencies in the range of 80–99%, including the BiOX/GaMOF S-scheme composite (96.27%) and the PAN@ZnONPs/Bio-MOF catalyst (99.22%). Across all evaluated studies, the median removal efficiency was approximately 95%, with the interquartile range typically falling between 85% and 100%.

*Light source*

Recent research has focused on visible light and direct sunlight active photocatalysts to use sustainable energy.

- **Visible light:** A considerable number of studies employed visible light sources to

facilitate the reaction, overcoming the wide bandgap limitations of traditional materials. Examples include $Nd_2O_3/TiO_2$ nanocomposites and $CoFe_2O_4/ZnO$ systems.

- **Sunlight:** Practical applicability was demonstrated by researchers using natural or simulated sunlight, such as Golmohammadi et al. for $Ag/SiO_2$ and Cilamkoti & Dutta for p-type $ZnO/N\text{-}SiO_2$ nanorods.
- **UV light:** UV irradiation is still highly effective for wide-bandgap semiconductors, utilized by systems like $TiO_2$ NTAs and ZnO NPs. A significant limitation in the current literature is the absence of Electrical Energy per Order (EEo) calculations. As indicated in Table 1, nearly all reviewed papers failed to report this metric. For photocatalysis to compete with traditional physicochemical treatments, future research must shift from reporting simple percentage removal to quantifying energy efficiency. Researchers are strongly encouraged to report EEo using the standard equation:

$$EEO = \frac{P \times t \times 1000}{V \times 60 \times \log\left(\frac{C0}{Cf}\right)}$$

Where P is the rated power of the system (kW), t is the time (min), V is the volume (L), and C0 and Cf are the initial and final concentrations.

*Kinetics*

The pseudo-first-order model mostly explains how CIP breaks down over time, yielding observable rate constants ($K_{obs}$). This model exhibited the optimal fit for data in several studies, including Tang et al. ($2.38 \times 10^{-2}$ $min^{-1}$ for PAN@ZnONPs/Bio-MOF) and Wei et al. (0.0486 $min^{-1}$ for $Bi_2MoO_6$/Banana Peel Biochar). Exceptionally rapid kinetics were also reported, such as 1.1 $min^{-1}$ for $TiO_2$ NTAs by Abromaitis et al. The degradation kinetics are strictly governed by structural design, dopants, light sources, and reaction conditions. Overall, the reported pseudo-first-order rate constants ($K_{obs}$) exhibited a wide range from 0.0034 to 1.1 $min^{-1}$, with a median value of approximately 0.035 $min^{-1}$.

*Stability and reusability of catalysts*

For photocatalysts to be economically viable and sustainable, they must be stable and reusable. Most studies looked at how well the catalyst worked over three to six consecutive cycles.

- **Structural stability:** Characterizations done after the reaction usually showed that the catalysts were structurally sound. For example, Wei et al. reported that $Bi_2MoO_6$/Banana Peel Biochar endured 5 cycles without efficiency loss, and the RGO-bridged $CuFe_2O_4@Ag_2S$ heterojunction demonstrated excellent reusability over six consecutive cycles.
- **Magnetic/Immobilized recovery:** Systems offering easy separation were highly beneficial for recovery. Radić et al. reported success using an IO-$TiO_2$ magnetic nanocomposite, and Borges et al. utilized supported $TiO_2$ on glass rings to sidestep the challenges of powder recovery.

*Degradation mechanisms and pathways*

The creation of highly reactive oxygen species (ROS) is what makes CIP break down through photocatalysis. A comprehensive overview of this process, illustrating the charge transfer pathways in an advanced heterojunction (e.g., S-scheme) and the subsequent generation of ROS for CIP degradation, is depicted in Figure 5.

- **Active species:** Radical scavenging experiments have consistently identified hydroxyl (OH) and superoxide ($O_2^{\bullet -}$) radicals, as well as photogenerated holes ($h^+$), as the primary species responsible for oxidizing the organic molecules. This was validated in research conducted by Tang et al. and El Golli et al (32, 41).
- **Charge transfer mechanisms:** New heterojunction designs have been put forward

to improve charge separation. Multiple studies confirmed S-scheme mechanisms (e.g., BiOX/GaMOF and N-CQDs/$TiO_2$) which maintain the elevated redox potential of the charge carriers.

- **Intermediates and pathways:** Analyses have clarified degradation pathways that include the cleavage of piperazine and quinolone rings, oxidation, and complete C-F cleavage. Studies like those by Dong et al. confirmed that the biotoxicity of CIP toward E. coli was eliminated following photocatalysis, yielding low-toxicity end products.
- **Chemical specificity of the degradation:** The structural advantage of advanced heterojunctions is directly linked to the chemical stability of ciprofloxacin. CIP possesses an incomplete biodegradability and a highly stable quinolone structure that hinders natural decomposition. Conventional treatment methods and simple single-component oxides often fail to generate ROS with sufficient oxidation potential to break these bonds efficiently. In contrast, advanced systems (e.g., S-scheme) preserve the high thermodynamic potential of photogenerated holes. These potent carriers are energetically capable of initiating ring-opening and defluorination, which are critical steps in CIP mineralization. This explains why heterojunctions consistently achieve strong mineralization capacity and non-toxic end products.

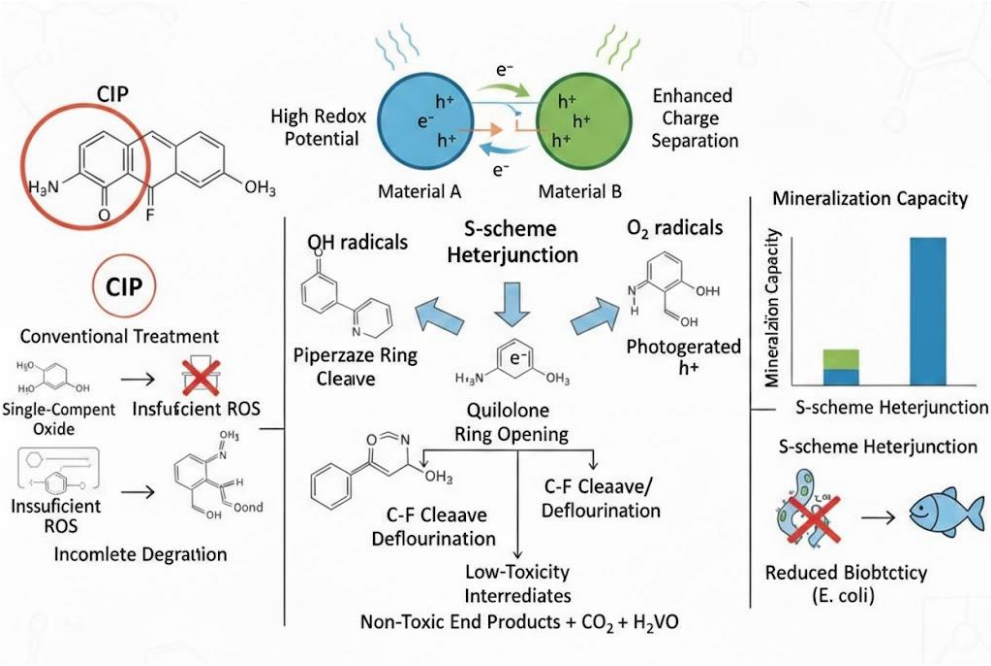


**Figure 5. Schematic representation of the charge transfer mechanism in an advanced S-scheme heterojunction and the generation of reactive oxygen species (•OH, $O_2$•$^-$, $h^+$) leading to the cleavage and mineralization of ciprofloxacin.**

*Critical challenges and knowledge gaps*

A systematic synthesis of the included studies reveals fundamental hurdles that limit the validity of current laboratory data for real-world applications:

- **The Mineralization paradox and intermediate toxicity:** A major discrepancy exists between parent compound removal and mineralization. While CIP removal efficiencies often exceed 90%, only about 35% of the reviewed studies explicitly quantified mineralization. Among these,

Total Organic Carbon (TOC) or Chemical Oxygen Demand (COD) removal rates vary significantly, sometimes only reaching 40-50%. This indicates the accumulation of transformation products. Future research must prioritize pathway analysis coupled with stringent toxicity assays rather than relying solely on removal rates.

- **Experimental matrix vs. real effluents:** The overwhelming majority of studies (over 90%) utilize synthetic aqueous environments, whereas fewer than 10% evaluated the photocatalysts in real wastewater or spiked environmental matrices, thereby ignoring the complex chemistry of real effluents. Consequently, the reported degradation efficiencies in laboratory settings likely overestimate the performance expected in real wastewater treatment applications.
- **Reactor configuration:** A significant portion of reviewed studies employ slurry-type batch reactors with powder catalysts. While effective for screening, this configuration faces massive bottlenecks in catalyst recovery and secondary pollution risks. Furthermore, the extreme heterogeneity in reported light sources without standardized metrics makes direct comparisons difficult.

## Conclusion

This systematic review evaluated photocatalytic approaches for degrading the antibiotic ciprofloxacin (CIP) in aqueous systems and identified operational variables that govern performance, including catalyst dosage, pH, initial CIP concentration, irradiation source, and contact time. Across the 69 selected studies, effective conditions commonly included catalyst dosages of approximately 0.1–1.0 g/L and reaction times of approximately 60–120 minutes, reflecting a trade-off between active-site availability and optical scattering at higher solid loading. The optimal pH was catalyst-dependent, although many advanced composites maintained strong performance near neutral to mildly alkaline conditions. Mechanistic improvements over the past decade have been consistent across platforms, including S-scheme and Z-scheme heterojunction construction, dopant engineering, and integration with sustainable supports such as biochar or fly ash to increase visible-light absorption and improve charge separation. These designs often achieve >90% CIP removal and frequently follow pseudo-first-order kinetics under the reported test regimes. Studies incorporating MS analysis and toxicity estimation indicate that degradation can proceed beyond parent depletion toward less toxic transformation products via quinolone and piperazine ring cleavage, with partial to complete mineralization reported in a subset of the literature.

This review shows that photocatalytic advanced oxidation processes are promising for the degradation of recalcitrant antibiotics like CIP in aqueous solutions. However, because a large number of research studies are carried out on a laboratory scale using synthetic wastewater, the results may not be directly scalable to pilot applications. Most current studies focus on powder catalysts, which pose challenges for recovery and reuse, although magnetic composites have shown promise in addressing these issues. Furthermore, the predominant use of slurry reactors in current research presents a significant bottleneck for downstream processing. To bridge the gap between laboratory success and industrial application, the focus must shift towards immobilized catalyst supports [e.g., coating on glass rings or membranes], EEo quantification, and the treatment of real effluents containing complex co-existing ions to provide a holistic understanding of antibiotic removal from aquatic environments.

**Table 1. Key characteristics of studies investigating the efficiency of photocatalytic processes for ciprofloxacin removal from aqueous environments**

| No. | Study specifications | Catalyst type | Operating conditions | | | | | CIP removal efficiency | $K_{obs}$ ($min^{-1}$) | Catalyst stability | Mineralization rate | Toxicity and degradation pathway | EEo (Kwh) | References |
|---|---|---|---|---|---|---|---|---|---|---|---|---|---|---|
| | | | pH | Cip (mg/L) | Dose (g/L) | Time (min) | Light Source | | | | | | | |
| 1 | Chen et al., 2025, China | BiOX/GaMOF (S-scheme) | 7 | 20 | 0.4 | 120 | UV | 96.27% | 0.369 | 95.79 | NR | Four pathways, toxicity reduction | NR | (42) |
| 2 | Mohamed et al., 2025, Egypt | NiO@g-$C_3N_4$ nanocomposite | 8 | 10 | 1 | 60 | sunlight | 78.5% | 0.025 | >50 % removal after 4 reuse cycles | Effective (S-scheme mechanism) | Not toxic; full photocatalytic oxidation suggested | NR | (35) |
| 3 | Ateş et al., 2024, Turkey | N-CQDs/$TiO_2$ (S-scheme) | 5 | 5 | 0.4 | 120 | UV-A | 91.8% | 0.0138 | NR | NR | S-scheme mechanism proposed | NR | (43) |
| 4 | Abromaitis et al., 2024, Lithuania | $TiO_2$ nanotubes (NTAs) | NR | 5-10 | NR | 8 | UV-C | 100% | 1.1 | 96.26% after 5th cycle | 57% TOC removal after 30 min | Log-5 bacterial reduction | NR | (37) |
| 5 | Cilamkoti & Dutta, 2024, India | p-type ZnO/N-$SiO_2$ nanorods | 6.3 | 12 | 0.4 | 90 | sunlight | 93% | 0.029 | 88% after 4th cycle | 80% degradation, not full mineralization | Two degradation pathways proposed | NR | (44) |
| 6 | Ecareño-Torres et al., 2024, Mexico | $TiO_2$/$SnO_2$/g-$C_3N_4$ (composite) | 6 | 10 | 1 | 300 (UV), 10 (sunlight) | UV and sunlight | 97.87% | 0.024 | High adsorption (≈ 30 %) + excellent photo-stability over cycles | Significant | Intermediate particles were analyzed, the pathway with reactive oxygen species | NR | (45) |
| 7 | Wei et al., 2024, China | $Bi_2MoO_6$/Banana Peel Biochar | 8 | 10 | 0.5 | 90 | Vis | 98.7 % | 0.0486 | 5 cycles without loss | 85 % | •OH, and $h^+$ dominant; toxicity reduction significantly by LC–MS analysis | NR | (46) |
| 8 | Baldez et al., 2024, Brazil | ZnO@FAU Composite | 7 | 10 | 0.16 | 90 | UV | 92% | NA | 3 cycles; 75.7 % | NR | $h^+$ is the dominant active species; •OH minor; direct | NR | (40) |

| | | | | | | | | | | | | | | |
|---|---|---|---|---|---|---|---|---|---|---|---|---|---|---|
| | | | | | | | | | | removal in cycle 3; FTIR unchanged | | oxidation by holes (and indirect via •OH); toxicity not evaluated | | |
| 9 | Radić et al., 2024, Croatia/Slovenia | IO-TiO2 magnetic nanocomposite | 7 | 8 | 0.2 | 150 | UV-B | 70 % | 0.0063 | Reused 4 times without activity loss | 60 % | Hydroxyl radical oxidation; no residual toxicity after treatment | NR | (47) |
| 10 | Tang et al., 2024, China | PAN@ZnONPs/Bio-MOF | 7.2 | 10 | 0.8 | 100 | Vis | 99.22 % | $2.38 \times 10^{-2}$ | Excellent (≥90 % efficiency after reuse) | TOC ≈ 50 % | $h^+$, •OH, $•O_2^-$ active; stable low-toxicity products | NR | (48) |
| 11 | Hayri-Senel et al., 2024, Turkey | PS-$TiO_2$ Composite | 3 | 5 | 0.8 | 180 | Vis | 95.01% | 0.0125 | Stable; reusable | 85 % (TOC basis) | •OH and $•O_2^-$ radicals; piperazine-ring cleavage | NR | (49) |
| 12 | El Golli et al., 2024, Italy | ZnO/g-$C_3N_4$ (Green Coating) | NR | 10 | NR | 210 | sunlight | 100 % | 0.02113 | High 89 % efficiency retained in second cycle | Near-complete decomposition confirmed by HPLC; no CIP peak after 210 min | •OH, and $O_2•^-$ radicals; major pathways: oxidation (+O), decarboxylation ($–CO_2$), H elimination | NR | (50) |
| 13 | Machín et al., 2024, Spain | 5% ($Co_3O_4$-g$C_3N_4$) @ZnONPs | 7 | 10 | 1.1 | 60 | sunlight | 99 % | NR | 6 % loss after 15 cycles | NR | By-products via superoxide radicals ($•O_2^-$ dominant) | NR | (51) |
| 14 | Fazil & Narayanan, 2023, India | 5Ag/ZnO (Mesoporous) | 6.5 - 7.5 | 25 | 0.2 | 240 | Vis | 76.7% | 0.0034 | Effective after 5 cycles | Not numerical but quinolone-ring breakdown confirmed by LC-MS | CIP quinolone ring cleavage observed → non-toxic products | NR | (52) |
| 15 | Golmohammadi et al., 2023, Iran | Ag/$SiO_2$ (Rice Husk Silica) | 6.7 | 40 | 0.6 | 180 | sunlight | 98% | $2.18\times10^{-2}$ | Stable after 3 cycles with no efficiency loss | TOC removal measured | Not toxic after treatment; decomposition confirmed | NR | (53) |
| 16 | Ngo et al., 2023, Vietnam | CuFe2O4/rGO/Halloysite | 7 | 20 | 0.2 | 60 | UV | 99 | 0.006332 | > 90 % after 4 runs | 78 % | Piperazine and quinolone oxidation → benign products | NR | (54) |
| 17 | Kumar, 2023, India | SnS2/BiVO4 nanocomposite | NR | 10 | 0.6 | 105 | sunlight | 92% | 0.0184 | Up to 5 cycles with acceptable efficiency, low % metal emission | Effective, confirmed (ROS generation) | Reduction of toxicity, decomposition pathway involving $•O2^-$ and h+, Z-scheme composition | NR | (55) |

| | | | | | | | | | | | | | | |
|---|---|---|---|---|---|---|---|---|---|---|---|---|---|---|
| 18 | Goudarzi et al., 2023, Iran | Mn-$Tl_2WO_4$ Nanostructures | 9 | 10 | 0.3 | 90 | UV | 76% | NR | Good, the performance decreased by only 1-3% after 3 reuse cycles | NR | A general photocatalytic mechanism involving reactive oxygen species is assumed | NR | (56) |
| 19 | Borges et al., 2023, Portugal | Batch Reactor: Powdered $TiO_2$ (Degussa P25) Packed Bed Reactor: Supported $TiO_2$ on glass rings/cylinders | NR (ambient) | 50 | NR | 200 | Sunlight | 95% | NR | reusable supported $TiO_2$ (glass rings > cylinders) | nearly complete under solar run | The general mechanism involving hydroxyl radicals (˙OH) is assumed; no specific scavenger tests were conducted | NR | (57) |
| 20 | García-Reyes et al., 2022, Spain | XGS-Fe-Im | NA | 15 | 1 | 60 | Sunlight | 60 % | 0.015 | > 90 % efficiency after 5 cycles | 80 % TOC removal | Superoxide and hydroxyl radicals dominate; non-toxic end-products | NR | (58) |
| 21 | Ahmadmoazzam et al., 2022, Iran | $Ag_2O$-AgI /$TiO_2$ | 9.5 | 10 | NA | 120 | Vis | 92.8% | 0.021 | Catalyst stayed stable for 6 days | 51% TOC removal | Proposed degradation pathway based on GC-MS reported | NR | (59) |
| 22 | Alam et al., 2022, Pakistan/Saudi Arabia/China | Mn/Co oxide nanocomposite | 4 | 3.31 | 1 | 120 | Sunlight | 56.3% | 7.9 x $10^{-2}$ | Stable for 5 cycles | NR | Identification of active species (•OH, $O_2^-$, $h^+$), reaction pathway identified | NR | (34) |
| 23 | Shawky & Alshaikh, 2022, Egypt/Saudi Arabia | 3% $CoFe_2O_4$/ZnO | NR | 10 | 2.4 | 45 | Vis | 100% | 0.103 | 97 % after 5 cycles | 85 % | Complete C–F cleavage → $CO_2$ + $H_2O$ (end non-toxic) | NR | (60) |
| 24 | Xiao et al., 2022, China | CNBN (Membrane Loaded) | 5.3 | 10 | 3.1-3.3 × $10^{-3}$ (g $cm^{-2}$) | 40 | sunlight | NR | 2.7 × $10^{-3}$ | Stable > 40 days use | > 80 % | Ring-opening + decarboxylation → low-toxicity products | NR | (61) |
| 25 | Alhaddad & Amin, 2022, Saudi Arabia | Pt@BiVO4-g-C3N4 | NR | NR | 2.4 | 90 | Vis | 100 % | NR | maintained after several reuse cycles | nearly complete decomposition confirmed | non-toxic intermediates confirmed via PL and photo-current tests | NR | (62) |
| 26 | Batterjee et al., 2022, Saudi Arabia | LP-ZnO NPs | 8 | 6.62 | 0.1 | 160 | UV | 83 | 0.011 | 5 cycles with high stability | NR | Dominant species: •OH, presence of $h^+$ and $•O_2^-$ also confirmed | NR | (63) |
| 27 | Thuan et al., 2022, Vietnam | 5% ZnO/g-$C_3N_4$ | 8 | 1 | 0.5 | 150 | Vis | 97.6% | 0.0281 | 89.8 % efficiency after 3 cycles (6 cycles tested) | NR | •OH, $•O_2^-$, $h^+$ active species; benign products | NR | (64) |
| 28 | Amir et al., 2022, Pakistan/Australia/ Korea | BCZ-3 | 7 | 100 | 1 | 240 | Vis | 98.5% | NA | BCZ-3 showed good stability, degrading 80.3% of CIP after four cycles. | 98.1% COD | Radicals break down CIP into intermediates (piperazinyl ring or quinolone part) and then into $CO_2$ and $H_2O$. | NR | (65) |

| | | | | | | | | | | | | | |
|---|---|---|---|---|---|---|---|---|---|---|---|---|---|
| 29 | Alhaddad et al., 2022, Saudi Arabia/Kuwait | $Nd_2O_3/TiO_2$ (1.5%) | NR | 10 | 2 | 150 | Vis | 100% | 0.0086 | It retained 93% of its efficiency after five consecutive cycles. | NR | Based on the reported scavenger test results. | NR | (66) |
| 30 | Beshkar et al., 2021, Iran | $Cu_2O/Cu_2(PO_4)$ (OH) | NR | 10-20 | 1 | 120 | sunlight | 98% | NA | 95% after 5 cycles | NR | p-n heterojunction mechanism | NR | (67) |
| 31 | Kaur et al., 2021, India | Ag-Fe-TiO2 Composite | 3.5 | 25 | 100% area covered (120 beads) | 60 | sunlight | 94.4% | 0.068 | Stable up to 30 reuse cycles | Confirmed via GC-MS intermediates | Detoxified; pathway verified by inhibition-zone test | NR | (68) |
| 32 | Alhaddad & Shawky, 2021, Saudi Arabia/Egypt/Japan | 3%FO@LNTO | NR | 10 | 2 | 90 | Vis | 100% | 0.047 | It showed remarkable stability, retaining nearly 95% efficiency after five cycles. | NR | Proposed photocatalytic mechanism reported | NR | (22) |
| 33 | Akbari et al., 2021, Iran/Spain | S, N-MgO | 9 | 50 | 0.1 | 30 | UV-A | 99% | 0.115 | The catalyst showed high stability, maintaining over 95% efficiency after four reuses. | The TOC removal, indicating mineralization, reached 92% after 90 minutes of reaction. | Degradation pathway based on LC/MS analysis reported | NR | (69) |
| 34 | Basaleh et al., 2021, Saudi Arabia and Egypt | 3% CdO/La-$NaTaO_3$ | NR | 10 | 2 | 90 | Vis | 100% | 0.049 | 97% after 5 cycles | NR | Production of active species •OH and $•O_2^-$, Z-scheme mechanism, complete mineralization | NR | (21) |
| 35 | Alshaikh et al., 2021, Saudi Arabia/Egypt/UK | 3 wt% $Co_3O_4$/ZnO | NR | 10 | 2.4 | 30 | Vis | 100% | 0.2 | The catalyst showed high stability, retaining 97.7% of its initial efficiency after five reuses | 93.3% TOC removal | Mechanism reported via Scavenger test and p-n heterojunction diagram | NR | (70) |
| 36 | Dong et al., 2021, China | PDI/rGO Composite Film | NR | 10 | 5% mass ratio film | 120 | Vis | 94.31 % | NR | excellent after 3 cycles | almost complete (3D-EEM fluorescence loss) | clean water similar to DI water; main radicals $h^+$ and $•O_2^-$ | NR | (71) |

| | | | | | | | | | | | | | | |
|---|---|---|---|---|---|---|---|---|---|---|---|---|---|---|
| 37 | Liu et al., 2021, China | $Fe_3O_4$@$SiO_2$@$Bi_2O_2CO_3$-Sepiolite | NR | 10 | 1 | 90 | vis | 92.1 % | 0.03823 | reusability & recyclability | Measured TOC removal (value not numerical) | NR | NR | (72) |
| 38 | Bouyarmane et al., 2021, Morocco | TiHAp Nanocomposite | 6.1 | 20 | 2 | 15 | UV | 100 % | 0.1765 | reusable after calcination 500 °C, no activity loss | High, with 98% COD (Chemical Oxygen Demand) removal after 2 hours | no bacterial inhibition post-treatment (E. coli, B. subtilis, S. aureus = 0 mm zones) | NR | (73) |
| 39 | Ahamad et al., 2021, Saudi Arabia/Korea/India | $FeWO_4$/NC-800 | 8 | 10 | NA | 100 | Vis/sunlight | 92.23% | 0.0240 | Good | TOC removal reached 65.08% after 100 minutes of irradiation | Degradation pathway reported via MS/MS and DFT calculations | NR | (74) |
| 40 | Alahmadi et al., 2020, Saudi Arabia/Egypt | 0.6 wt.% Pt@ZnO nanorods | NR | 10 | 1.6 | 75 | Vis | 100% | NR | 98% after 5th cycle | NR | Complete decomposition, referring to hydroxyl radicals and electron transfer | NR | (75) |
| 41 | Balta et al., 2020, Turkey/Slovakia | WTC9 | 6.3 | 10 | 0.4 | 60 | Sunlight | 96% | 0.058 | NR | NR | Only charge transfer mechanism reported | NR | (76) |
| 42 | Alhaddad et al., 2020, Saudi Arabia/Egypt | 7wt% $ZnMn_2O_4$ZnO | NR | 10 | 1.5 | 30 | Vis | 100% | NR | remarkable stability, with its efficiency remaining almost unchanged after five reuses | NR | only charge transfer | NR | (77) |
| 43 | Bai et al., 2020, China | $Bi_2WO_6$/CuS/g-$C_3N_4$ | NR | 10 | 0.1 | 75 | Vis | 74.94% | 0.026 | 72.47% after 4th cycle | Mineralization suggested, not quantified | Active species $e^-$, $h^+$, $O_2^-$, complete decomposition pathway identified | NR | (78) |
| 44 | Jiménez-Salcedo et al., 2020, Spain | g-C3N4 Nanocomposite | NR | 4 | 0.22 | 150 | Vis | 100% | 0.035 | Stable, reusable | Partial; eight intermediat | Piperazine-ring attack by •OH → defluorination → $CO_2$ + $H_2O$ + $NO_3^-$ + $F^-$ | NR | (79) |

| | | | | | | | | | | | | | | |
|---|---|---|---|---|---|---|---|---|---|---|---|---|---|---|
| | | | | | | | | | | es identified | | | | |
| 45 | Shoueir et al., 2020, Egypt | PAN@ZnONPs/Bio-MOF | NR | 5 | 0.32 | 70 | Vis | 97.2% | 0.0503 | Maintained > 95 % for 4 cycles | 80 % (TOC) | C–F and piperazine cleavage → $CO_2$ + $H_2O$ (end non-toxic) | NR | (27) |
| 46 | Ulyankina et al., 2020, Russia | ZnO NPs (Periodic Electrochemical) | 6.5 | 5 | 0.5 | 30 | UV | 93.6 % | NR | Good (ZnO – LiCl synthesis route) | TOC 51 % | $h^+$ dominant; low toxicity confirmed | NR | (80) |
| 47 | Huang et al., 2020, China | $TiO_2$@AMSF | 6-7 | 50 | 0.2 | 400-450 | UV | 153 (mg/g) | $2.1\times10^{-4}$ | Reusable 3 cycles | COD ≈ 70 % | Hydroxyl + superoxide radicals, “capture & destroy” mechanism | NR | (31) |
| 48 | Tahir et al., 2020, Pakistan/Saudi Arabia | $Bi_2WO_6$/PANI (5%) | 4 | 10 | 0.5 | 90 | Vis | 98% | 0.041050 | The catalyst showed good stability after four reuse cycles. | NR | Degradation pathway based on HPLC/MS analysis reported | NR | (81) |
| 49 | Dong et al., 2020, China | ZSO-C | 5.9 | 10 | 0.5 | 100 | sunlight | 85.9% | $1.93 \times 10^{-2}$ | retained > 90 % activity after 4 cycles | onfirmed nearly complete by TOC reduction | Biotoxicity of CIP toward E. coli eliminated after photocatalysis | NR | (82) |
| 50 | Durán-Álvarez et al., 2019, Mexico | AgBr/Ag/Bi2WO6 (Z-scheme) | 7 | 30 | 0.5 | 300 | Vis | 57.6 | NR | Stable after 4 cycles | 38 % TOC (pure water); complete mineralization (tap water) | degradation into non-toxic products, pathway determined by LC-MS | NR | (39) |
| 51 | Malakootian et al., 2019, Iran | $ZnFe_2O_4$@CMC | 7 | 5 | 1 | 100 | UV-C | 87 % | 0.43 | Excellent after five runs | 75 % TOC | Complete mineralization to $CO_2$ + $H_2O$ confirmed | NR | (83) |
| 52 | Yan et al., 2019, China | CNT@MIL-101(Fe) | 3 | 1 | 0.5 | 45 | Vis | 90 % | 0.0411 | Fe leaching ≈ 50 % lower than MIL-101(Fe) | NR | •OH, oxidation dominant, low-toxicity end products | NR | (84) |
| 53 | Behera et al., 2019, India | ZFO@3%RGO | NA | 20 | 1 | 60 | Sunlight | 73.4% | 0.021 | Catalyst stability was tested over four cycles. | NA | Mechanism reported based on Scavenger, NBT, and TA tests | NR | (85) |
| 54 | Nasiri et al., 2019, Iran | CuFe2O4@methylcellulose | 7 | 3 | 0.67 | 90 | UV-C | 80.74 % | 0.0184 | 4 cycles, ferromagnetic separation | 68.26 % COD | Radical oxidation (•OH), non-toxic residues | NR | (86) |
| 55 | Hassani et al., 2018, Iran/Turkey | TiO2/MMT nanocomposite | 7.16 | 25.80 | 0.07 | 29.48 | UV-A | 95.78% | NR | NR | high (near-complete) | •OH, $O2^-$, homogeneous and heterogeneous mechanisms of photocatalysis+ozone | NR | (87) |

| | | | | | | | | | | | | | | |
|---|---|---|---|---|---|---|---|---|---|---|---|---|---|---|
| 56 | Khoshnamvand et al., 2018, Iran | CuO Nanoparticles | 8.17 | 11.2 | 0.08 | 60 | UV-C | 98.9% | NR | NR | Based on COD removal | NA | NR | (88) |
| 57 | Xing et al., 2018, China | N-$TiO_2$/Glass Spheres | 7 | 20 | 3 | 90 | Vis | 93.5% | 0.02859 | >90 % activity after 5 cycles | NR | 7 degradation products detected; toxicity reduced | NR | (89) |
| 58 | Eskandari et al., 2018, Iran | Synthetic ZnO | 5 | 10 | 0.15 | 140 | UVC | 100% | 0.037 | High (reusable) | NR | no interference from anions ($Cl^-$, $SO_4^{2-}$, etc.) | NR | (90) |
| 59 | El Bekkali et al., 2018, Morocco/France | 25ZnHAp / 40ZnHAp | NR | 20 | 2 | 20 | UV A-B-C | 100% | NR | NR | CIP disappeared quickly; intermediates likely stayed on the surface, showing degradation but incomplete mineralization | Proposed degradation pathway based on HPLC data reported | NR | (91) |
| 60 | Das et al., 2018, India/Sweden | Fe-ZnO nanoparticles | 9 | 10 | 0.15 | 210 | sunlight | 100 % | NA | Stable under sunlight; reusable | NA | Hydroxyl radical (•OH) and Fenton process | NR | (92) |
| 61 | Sayed et al., 2018, Pakistan/China | PVA-assisted TiO2/Ti + PMS | 6.3 | 5 | NR | 60 | sunlight | 98.3% | 0.0582 | > 90 % after 5 cycles | 82 % (TOC) | C7–N and piperazine bond cleavage → non-toxic products | NR | (93) |
| 62 | Kumar et al., 2017, India | RPC | 6.1 | 20 | 1 | 90 | sunlight | 92.8% | 0.026 | 5 reuse cycles-efficiency dropped slightly from 91.8 → 86.4 % | 44 % COD | Non-toxic intermediates; •OH and $O_2^{\bullet-}$ radicals dominate oxidation Pathway leads to ring-opened carboxylic acids and $CO_2$ | NR | (94) |
| 63 | Bojer et al., 2017, Denmark | Mesostructured ZnO Nanotubes | 8 | $2\times 10^{-5}$ ($Mol.L^{-1}$) | 14 (mg) | 120 | sunlight | 12% | $9.61\times 10^{-4}$ | no catalyst loss in flow operation | confirmed by UV–Vis complete removal | not tested (only noted environmental relevance) | NR | (95) |
| 64 | Genç, 2016, Turkey | $TiO_2$ | 9 | 10 | 0.8 | 30 | UV | 97.1 % | 0.445 | NR | 40.3% COD | Two-stage oxidation → non-toxic acids (1,4-benzenedicarboxylic acid, etc.) | NR | (96) |
| 65 | Zhang et al., 2015, China | BiOBr | 9 | 5 | 0.5 | 140 | Vis | 100 % | 0.037 | $Bi^{3+}$ leaching < 2 % after 30 h | TOC 40 % | Low toxicity; main intermediate = desethylene CIP | NR | (97) |
| 66 | Lima et al., 2014, Portugal | Fe2+ (homogeneous) / Magnetite nanoparticles (heterogeneous) | 2.8 and 6.8 | 10 | 4 and 0.004 | 1.8 | sunlight | 85% and 55% | NR | Stable, easily magnetically recovered | NR | •OH, radical oxidation; non-toxic effluent | NR | (98) |

| | | | | | | | | | | | | | | |
|---|---|---|---|---|---|---|---|---|---|---|---|---|---|---|
| 67 | Paul et al., 2010, United Kingdom | $TiO_2$ Hombikat UV100 (Anatase) | 6 | 33.1 | 0.5 | 25 | UV-A | >99% | NA | NR | $NH_3$ and $F^-$ released; partial mineralization | Transformation products had negligible antibacterial activity | NR | (99) |
| 68 | El-Kemary et al., 2010, Egypt | ZnO nanoparticles | 10 | 5 | 0.02 | 60 | UV | 50% | 0.004 ±3 0.0023 | NR | NR | Removal of functional groups, route based on optical decomposition | NR | (36) |
| 69 | An et al., 2010, China | $TiO_2$ Degussa P25 | 9 | 33.1 | 1.5 | 30 | UV | 99% | 0.38 | NR | NR | Direct photo-hole oxidation and hydroxyl radical (˙OH) attack. Seven intermediates were identified | NR | (100) |

**Funding Source**

The authors did not receive support from any organization for the submitted work.

**Competing interests**

The authors declare that they have no known competing financial interests or personal relationships that could have appeared to influence the work reported in this paper.

**References**

1. Ngqwala NP, Muchesa P. Occurrence of pharmaceuticals in aquatic environments: A review and potential impacts in South Africa. South African Journal of Science. 2020;116(7-8):1–7.
2. Kayode-Afolayan SD, Ahuekwe EF, Nwinyi OC. Impacts of pharmaceutical effluents on aquatic ecosystems. Scientific African. 2022;17:e01288.
3. Al-Howri BM, Ismail S, Khajavian M. comprehensive review of ciprofloxacin pollution in water: sources, environmental impacts, remediation techniques, and research challenges. Environmental Monitoring and Assessment. 2025;197(10):1095.
4. Gauba P, Saxena A. Ciprofloxacin properties, impacts, and remediation. CABI Reviews. 2023(2023).
5. Nas B, Dolu T, Koyuncu S. Behavior and removal of ciprofloxacin and sulfamethoxazole antibiotics in three different types of full-scale wastewater treatment plants: a comparative study. Water, Air, & Soil Pollution. 2021;232(4):127.
6. Mathai T, Pal T, Prakash N, Mukherji S. Portable biosensor for the detection of Enrofloxacin and Ciprofloxacin antibiotic residues in food, body fluids, environmental and wastewater samples. Biosensors and Bioelectronics. 2023;237:115478.
7. Fu J, Huang C-H, Dang C, Wang Q. A review on treatment of disinfection byproduct precursors by biological activated carbon process. Chinese Chemical Letters. 2022;33(10):4495–504.
8. Wu H, Li L, Wang S, Zhu N, Li Z, Zhao L, et al. Recent advances of semiconductor photocatalysis for water pollutant treatment: mechanisms, materials and applications. Physical Chemistry Chemical Physics. 2023;25(38):25899–924.
9. Roslan NN, Lau HLH, Suhaimi NAA, Shahri NNM, Verinda SB, Nur M, et al. Recent advances in advanced oxidation processes for degrading pharmaceuticals in wastewater—a review. Catalysts. 2024;14(3):189.
10. Krystynik P. Advanced oxidation processes (AOPs)–utilization of hydroxyl radical and singlet oxygen. Reactive oxygen species: IntechOpen; 2021.
11. Wang L, Li Y, Zhao L, Qi Z, Gou J, Zhang S, et al. Recent advances in ultrathin two-dimensional materials and biomedical applications for reactive oxygen species generation and scavenging. Nanoscale. 2020;12(38):19516–35.
12. Chida T, Sasaki S, Hiromori K, Shibasaki-Kitakawa N, Kaneko T, Takahashi A. Insight into the generation network of reactive oxygen species in H2O under nonthermal atmospheric-pressure plasma irradiation using a kinetic modeling approach. Chemical Engineering Journal. 2024;501:157640.
13. NAGABHOOSHANAM N, SRIVANI B, VALLI B, KUMAR CP, LAL B, PRIYA D, et al. PHOTOCATALYTIC OXIDATION OF HAZARDOUS PETROCHEMICAL COMPOUNDS USING TiO 2 UNDER UV IRRADIATION. Oxidation Communications. 2025;48(2).
14. Navidpour AH, Abbasi S, Li D, Mojiri A, Zhou JL. Investigation of advanced oxidation process in the presence of TiO2 semiconductor as photocatalyst: property, principle, kinetic analysis, and photocatalytic activity. Catalysts. 2023;13(2):232.
15. Peiris S, de Silva HB, Ranasinghe KN, Bandara SV, Perera IR. Recent development and future prospects of TiO2 photocatalysis. Journal of the Chinese Chemical Society. 2021;68(5):738–69.
16. Lettieri S, Pavone M, Fioravanti A, Santamaria Amato L, Maddalena P. Charge carrier processes and optical properties in TiO2 and TiO2-based heterojunction photocatalysts: A review. Materials. 2021;14(7):1645.
17. Khan R, Rahman N, Prasannan A, Ganiyeva K, Chakrabortty S, Sangaraju S. Phase transition and bandgap modulation in TiO2 nanostructures for enhanced visible-light activity and environmental applications. Scientific Reports. 2025;15(1):20309.
18. Ahad A, Podder J, Saha T, Das HN. Effect of chromium doping on the band gap tuning of titanium dioxide thin films for solar cell applications. Heliyon. 2024;10(1).
19. Nair RV, Gummaluri VS, Matham MV, C V. A review on optical bandgap engineering in TiO2 nanostructures via doping and intrinsic vacancy modulation towards visible light applications. Journal of Physics D: Applied Physics. 2022;55(31):313003.
20. Velmurugan S, Jothi KJ, Pakrudheen I, Nagarani S, Mubarak S, Devanesan S, et al. Template-free synthesis of the highly ordered, efficient nano Nd2O3-TiO2 for visible-light-driven photocatalytic degradation of Rhodamine B. Ceramics International. 2025;51(5):6627–40.
21. Basaleh AS, Shawky A, Zaki ZI. La-doped NaTaO3 nanoparticles: Sol-gel synthesis and

synergistic effect of CdO decoration toward efficient visible-light degradation of ciprofloxacin in water. CERAMICS INTERNATIONAL. 2021;47(15):21350–7.

22. Alhaddad M, Shawky A. La-doped NaTaO3 perovskite nanocrystals supported with α-Fe2O3 for sustainable visible-light-driven elimination of ciprofloxacin in water. CERAMICS INTERNATIONAL. 2021;47(8):10688–95.

23. Bronzato JD, Bronzato JD, Brito AMM, Bettini J, Passini MRZ, Gomes BPFA, et al. Degradation of ciprofloxacin by green cobalt oxide quantum dots. Applied Surface Science. 2023;609.

24. Amariei G, Valenzuela L, Iglesias-Juez A, Rosal R, Visa M. ZnO-functionalized fly-ash based zeolite for ciprofloxacin antibiotic degradation and pathogen inactivation. JOURNAL OF ENVIRONMENTAL CHEMICAL ENGINEERING. 2022;10(3).

25. Beigi F, Mahjoub AR, Khavar AHC. Design and synthesis of Bi-doped NiAl-LDH/g-C3N4 heterostructure; a novel 2D/2D system for simultaneous enhanced photocatalytic degradation and fluorescence sensing of ciprofloxacin. APPLIED SURFACE SCIENCE. 2023;637.

26. Azqandi M, Nateq K, Golrizkhatami F, Nasseh N, Seyedi N, Mazari Moghaddam NSM, et al. Innovative RGO-bridged S-scheme CuFe2O4@Ag2S heterojunction for efficient Sun-light-driven photocatalytic disintegration of Ciprofloxacin. Carbon. 2025;231.

27. Shoueir K, Wassel AR, Ahmed MK, El-Naggar ME. Encapsulation of extremely stable polyaniline onto Bio-MOF: Photo-activated antimicrobial and depletion of ciprofloxacin from aqueous solutions. JOURNAL OF PHOTOCHEMISTRY AND PHOTOBIOLOGY A-CHEMISTRY. 2020;400.

28. Ates Y, Eroglu Z, Açisli Ö, Metin Ö, Karaca S. Exploring the efficiency of nitrogenated carbon quantum dots/TiO2 S-scheme heterojunction in photodegradation of ciprofloxacin in aqueous environments. TURKISH JOURNAL OF CHEMISTRY. 2024;48(4).

29. Chen P, Zhu Z, Liu Z, Liang F, Zhu X, Bin Z, et al. Efficient removal of ciprofloxacin from water by BiOX/GaMOF S-scheme heterojunction: A synergistic effect of adsorption and photocatalysis. Chemical Engineering Journal. 2025;506.

30. Wei YZ, Wang JH, Ma JK, Kong F, Xue JJ, Ye ZL, et al. Fabrication of porous biochar supported Bi2MoO6 photocatalyst for efficient degradation of ciprofloxacin in seawater under visible light irradiation: Mechanistic investigation and intermediates analysis. SEPARATION AND PURIFICATION TECHNOLOGY. 2024;349.

31. Huang XL, Wu S, Tang SZ, Huang L, Zhu DF, Hu Q. Photocatalytic hydrogel layer supported on alkali modified straw fibers for ciprofloxacin removal from water. JOURNAL OF MOLECULAR LIQUIDS. 2020;317.

32. Tang Q, He J, Fu Q, Zhao L, Tang H, Xie L, et al. Enhanced photocatalytic degradation performance of cornstalk templated TiO2 towards ciprofloxacin in hospital wastewater by the synergistic effect of the (101)/(001) facets coexposed and NiO cocatalyst. Journal of Alloys and Compounds. 2024;992.

33. Hayri-Senel T, Kahraman E, Sezer S, Aydin N, Nasun-Saygili G. Photocatalytic degradation of ciprofloxacin from water with waste polystyrene and TiO2 composites. Heliyon. 2024;10(3).

34. Alam A, Rahman WU, Rahman ZU, Khan SA, Shah Z, Shaheen K, et al. Photocatalytic degradation of the antibiotic ciprofloxacin in the aqueous solution using Mn/Co oxide photocatalyst. Journal of Materials Science: Materials in Electronics. 2022;33(7):4255–67.

35. Mohamed SK, Elhgrasi AM, Ali OI. Synergistic Adsorption-Photocatalysis Under Sunlight Irradiation of NiO/Graphitic Carbon Nitride Nanocomposite for the Removal of Ciprofloxacin from Wastewater. JOURNAL OF CLUSTER SCIENCE. 2025;36(2).

36. El-Kemary M, El-Shamy H, El-Mehasseb I. Photocatalytic degradation of ciprofloxacin drug in water using ZnO nanoparticles. JOURNAL OF LUMINESCENCE. 2010;130(12):2327–31.

37. Abromaitis V, Oghenetejiro O, Sulciute A, Urniezaite I, Sinkeviciute D, Zmuidzinaviciene N, et al. TiO2 2 nanotube arrays photocatalytic ozonation for the removal of antibiotic ciprofloxacin from the effluent of a domestic wastewater treatment plant: Towards the process upscaling. JOURNAL OF WATER PROCESS ENGINEERING. 2024;63.

38. Huang X, Wu S, Tang S, Huang L, Zhu D, Hu Q. Photocatalytic hydrogel layer supported on alkali modified straw fibers for ciprofloxacin removal from water. Journal of Molecular Liquids. 2020;317.

39. Durán-Álvarez JC, Méndez-Galván M, Lartundo-Rojas L, Rodríguez-Varela M, Ramírez-Ortega D, Guerrero-Araque D, et al. Synthesis and Characterization of the All Solid Z-Scheme Bi2WO6/Ag/AgBr for the Photocatalytic Degradation of Ciprofloxacin in Water. Topics in Catalysis. 2019;62(12-16):1011–25.

40. Baldez WMC, Santos J, Santos WDC, Aguilar-Pliego J, Martín N, Cabral AA, et al. Enhanced photodegradation of ciprofloxacin antibiotic using ZnO@FAU composite: A promising material for contaminant removal. DESALINATION AND WATER TREATMENT. 2024;318.

41. El Golli A, Fendrich M, Bajpai OP, Bettonte M, Edebali S, Orlandi M, et al. Parabolic trough concentrator design, characterization, and application: solar wastewater purification targeting textile industry dyes and pharmaceuticals-techno-economic study. EURO-MEDITERRANEAN JOURNAL FOR ENVIRONMENTAL INTEGRATION. 2024;9(4):1907–19.

42. Alduhaish O, Suganya G, Alajmi A, Sadeq AM, Praveen P, K K, et al. A novel binary bismuth molybdate-perovskite type Strontium Niobate for efficient photocatalytic degradation of ciprofloxacin. Journal of the Taiwan Institute of Chemical Engineers. 2025;167.

43. Ates Y, Eroğlu Z, Acisli Ö, Metin Ö, Karaca S. Exploring the efficiency of nitrogenated carbon quantum dots/TiO2 S-scheme heterojunction in the photodegredation of ciprofloxacin in aqueous environments. Turkish Journal of Chemistry. 2024;48(4):550–67.

44. Cilamkoti V, Dutta RK. Surface Modification of p-type ZnO Nanorods by Nitrogen Doped SiO2 Dots as an Efficient Solar Photocatalyst for Degradation of Ciprofloxacin in Water. ADVANCED SUSTAINABLE SYSTEMS. 2024;8(8).

45. Escareño-Torres GA, Pinedo-Escobar JA, De Haro-Del Río DA, Becerra-Castañeda P, Araiza DG, Inchaurregui-Méndez H, et al. Enhanced degradation of ciprofloxacin in water using ternary photocatalysts TiO(2)/SnO(2)/g-C(3)N(4) under UV, visible, and solar light. Environ Sci Pollut Res Int. 2024;31(28):40174–89.

46. Wei Y, Wang J, Ma J, Kong F, Xue J, Ye Z, et al. Fabrication of porous biochar supported Bi2MoO6 photocatalyst for efficient degradation of ciprofloxacin in seawater under visible light irradiation: Mechanistic investigation and intermediates analysis. Separation and Purification Technology. 2024;349.

47. Radic J, Zerjav G, Jurko L, Boskovic P, Zemljic LF, Vesel A, et al. First Utilization of Magnetically-Assisted Photocatalytic Iron Oxide-TiO2 Nanocomposites for the Degradation of the Problematic Antibiotic Ciprofloxacin in an Aqueous Environment. MAGNETOCHEMISTRY. 2024;10(9).

48. Tang QY, He J, Fu QC, Zhao LX, Tang H, Xie LX, et al. Enhanced photocatalytic degradation performance of cornstalk templated TiO2 towards ciprofloxacin in hospital wastewater by the synergistic effect of the (101)/(001) facets coexposed and NiO cocatalyst. JOURNAL OF ALLOYS AND COMPOUNDS. 2024;992.

49. Hayri-Senel T, Kahraman E, Sezer S, Erdol-Aydin N, Nasun-Saygili G. Photocatalytic degradation of ciprofloxacin from water with waste polystyrene and TiO2 composites. HELIYON. 2024;10(3).

50. El Golli A, Losa D, Gioia C, Fendrich M, Bajpai OP, Jousson O, et al. Advancing solar wastewater treatment: A photocatalytic process via green ZnO/g-C3N4 coatings and concentrated sunlight - Comprehensive insights into ciprofloxacin antibiotic inactivation. JOURNAL OF ENVIRONMENTAL MANAGEMENT. 2024;371.

51. Machín A, Morant C, Soto-Vázquez L, Resto E, Ducongé J, Cotto M, et al. Synergistic Effects of Co3O4-gC3N4-Coated ZnO Nanoparticles: A Novel Approach for Enhanced Photocatalytic Degradation of Ciprofloxacin and Hydrogen Evolution via Water Splitting. MATERIALS. 2024;17(5).

52. Fazil AA, Narayanan S. BAGSPl of mesoporous Ag/ZnO nanostructures for visible light mediated photocatalytic removal of ciprofloxacin from water; a morphological perspective. INORGANIC CHEMISTRY COMMUNICATIONS. 2023;154.

53. Golmohammadi M, Hanafi-Bojd H, Shiva M. Photocatalytic degradation of ciprofloxacin antibiotic in water by biosynthesized silica supported silver nanoparticles. CERAMICS INTERNATIONAL. 2023;49(5):7717–26.

54. Ngo HS, Nguyen TL, Tran NT, Le HC. Photocatalytic Removal of Ciprofloxacin in Water by Novel Sandwich-like CuFe2O4 on rGO/Halloysite Material: Insights into Kinetics and Intermediate Reactive Radicals. Water (Switzerland). 2023;15(8).

55. Kumar G. Sunlight Responsive 2D/2D SnS2/BiVO4 Nanocomposite for Photocatalytic Removal of Ciprofloxacin Antibiotic from Aqueous Medium. JOURNAL OF INORGANIC AND ORGANOMETALLIC POLYMERS AND MATERIALS. 2023;33(9):2710–20.

56. Goudarzi M, Hamzah Abdulhusain Z, Salavati-Niasari M. Low-cost and eco-friendly synthesis of Mn-doped Tl2WO4 nanostructures for efficient visible light photocatalytic degradation of antibiotics in water. Solar Energy. 2023;262.

57. Borges ME, de Paz Carmona H, Gutiérrez M, Esparza P. Photocatalytic Removal of Water Emerging Pollutants in an Optimized Packed Bed Photoreactor Using Solar Light. Catalysts. 2023;13(6).

58. García-Reyes CB, Salazar-Rábago JJ, Sanchez-Polo MS, Ramos VC. Synthesis and Use of Silica Xerogels Doped with Iron as a Photocatalyst to Pharmaceuticals Degradation in Water. Catalysts. 2022;12(11).

59. Ahmadmoazzam M, Takdastan A, Neisi K, Ahmadi M, Jorfi S, Babaei A. Photocatalytic degradation of ciprofloxacin by a novel visible light activated Ag2O-AgI/TiO2 nanocomposite: Activity, kinetic, mineralization and continuous-flow stability

test. INTERNATIONAL JOURNAL OF ENVIRONMENTAL ANALYTICAL CHEMISTRY. 2024;104(9):2096–115.

60. Shawky A, Alshaikh H. Cobalt ferrite-modified sol-gel synthesized ZnO nanoplatelets for fast and bearable visible light remediation of ciprofloxacin in water. ENVIRONMENTAL RESEARCH. 2022;205.

61. Xiao Z, Zheng Y, Chen P, Liu H, Fang Z, Zhang J, et al. Photocatalytic degradation of ciprofloxacin in freshwater aquaculture wastewater by a CNBN membrane: mechanism, antibacterial activity, and cyclability. Environmental Science: Nano. 2022;9(8):3110–25.

62. Alhaddad M, Amin MS. Removal of ciprofloxacin applying Pt@BiVO4-g-C3N4 nanocomposite under visible light. OPTICAL MATERIALS. 2022;124.

63. Batterjee MG, Nabi A, Kamli MR, Alzahrani KA, Danish EY, Malik MA. Green Hydrothermal Synthesis of Zinc Oxide Nanoparticles for UV-Light-Induced Photocatalytic Degradation of Ciprofloxacin Antibiotic in an Aqueous Environment. CATALYSTS. 2022;12(11).

64. Thuan DV, Nguyen TBH, Pham TH, Kim J, Chu TTH, Nguyen MV, et al. Photodegradation of ciprofloxacin antibiotic in water by using ZnO-doped g-C3N4 photocatalyst. CHEMOSPHERE. 2022;308.

65. Amir M, Fazal T, Iqbal J, Din AA, Ahmed A, Ali A, et al. Integrated adsorptive and photocatalytic degradation of pharmaceutical micropollutant, ciprofloxacin employing biochar-ZnO composite photocatalysts. JOURNAL OF INDUSTRIAL AND ENGINEERING CHEMISTRY. 2022;115:171–82.

66. Alhaddad M, Ismail AA, Alghamdi YG, Al-Khathami ND, Mohamed RM. Fabrication of novel neodymium oxide coupled mesoporous titania for effective visible light-induced photocatalyst for decomposition of Ciprofloxacin. OPTICAL MATERIALS. 2022;131.

67. Beshkar F, Salavati-Niasari M, Amiri O. Facile One-Pot In Situ Synthesis and Characterization of a Cu2O/Cu2(PO4)(OH) Binary Heterojunction Nanocomposite for the Efficient Photocatalytic Degradation of Ciprofloxacin from Aqueous Solution under Direct Sunlight Irradiation. INDUSTRIAL & ENGINEERING CHEMISTRY RESEARCH. 2021;60(26):9578–91.

68. Kaur N, Verma A, Thakur I, Basu S. In-situ dual effect of Ag-Fe-TiO2 composite for the photocatalytic degradation of Ciprofloxacin in aqueous solution. CHEMOSPHERE. 2021;276.

69. Akbari S, Moussavi G, Giannakis S. Efficient photocatalytic degradation of ciprofloxacin under UVA-LED, using S,N-doped MgO nanoparticles: Synthesis, parametrization and mechanistic interpretation. JOURNAL OF MOLECULAR LIQUIDS. 2021;324.

70. Alshaikh H, Shawky A, Mohamed RM, Knight JG, Roselin LS. Solution-based synthesis of Co3O4/ZnO p-n heterojunctions for rapid visible-light-driven oxidation of ciprofloxacin. JOURNAL OF MOLECULAR LIQUIDS. 2021;334.

71. Dong S, Zhao Y, Yang J, Liu X, Li W, Zhang L, et al. Visible-light responsive PDI/rGO composite film for the photothermal catalytic degradation of antibiotic wastewater and interfacial water evaporation. Applied Catalysis B: Environmental. 2021;291.

72. Liu L, Su G, Liu X, Dong W, Niu M, Kuang Q, et al. Fabrication of magnetic core–shell Fe3O4@SiO2@Bi2O2CO3–sepiolite microspheres for the high-efficiency visible light catalytic degradation of antibiotic wastewater. Environmental Technology and Innovation. 2021;22.

73. Bouyarmane H, El-Bekkali C, Labrag J, Es-Saidi I, Bouhnik O, Abdelmoumen H, et al. Photocatalytic degradation of emerging antibiotic pollutants in waters by TiO2/Hydroxyapatite nanocomposite materials. Surfaces and Interfaces. 2021;24.

74. Ahamad T, Naushad M, Alshehri SM. Analysis of degradation pathways and intermediates products for ciprofloxacin using a highly porous photocatalyst. CHEMICAL ENGINEERING JOURNAL. 2021;417.

75. Alahmadi N, Amin MS, Mohamed RM. Superficial visible-light-responsive Pt@ZnO nanorods photocatalysts for effective remediation of ciprofloxacin in water. JOURNAL OF NANOPARTICLE RESEARCH. 2020;22(8).

76. Balta Z, Simsek EB, Berek D. Promoting the photocatalytic removal rate of ciprofloxacin antibiotic over carbon fiber decorated tungsten trioxide/titanium dioxide catalysts. CHEMICAL ENGINEERING COMMUNICATIONS. 2022;209(1):108–17.

77. Alhaddad M, Mohamed RM. Synthesis and characterizations of ZnMn2O4-ZnO nanocomposite photocatalyst for enlarged photocatalytic oxidation of ciprofloxacin using visible light irradiation. APPLIED NANOSCIENCE. 2020;10(7):2269–78.

78. Bai Y, Mao W, Wu Y, Gao Y, Wang T, Liu S. Synthesis of novel ternary heterojunctions via Bi2WO6 coupling with CuS and g-C3N4 for the highly efficient visible-light photodegradation of ciprofloxacin in wastewater. Colloids and Surfaces A: Physicochemical and Engineering Aspects. 2021;610.

79. Jiménez-Salcedo M, Monge M, Tena MT. Study of intermediate by-products and mechanism of the photocatalytic degradation of ciprofloxacin in water using graphitized carbon nitride nanosheets. CHEMOSPHERE. 2020;247.

80. Ulyankina A, Molodtsova T, Gorshenkov M, Leontyev I, Zhigunov D, Konstantinova E, et al. Photocatalytic degradation of ciprofloxacin in water at nano-ZnO prepared by pulse alternating current electrochemical synthesis. JOURNAL OF WATER PROCESS ENGINEERING. 2021;40.

81. Bilal Tahir MB, Nawaz T, Nabi G, Sagir M, Rafique M, Ahmed A, et al. Photocatalytic degradation and hydrogen evolution using bismuth tungstate based nanocomposites under visible light irradiation. International Journal of Hydrogen Energy. 2020;45(43):22833–47.

82. Dong S, Cui L, Zhang W, Xia L, Zhou S, Russell CK, et al. Double-shelled ZnSnO3 hollow cubes for efficient photocatalytic degradation of antibiotic wastewater. Chemical Engineering Journal. 2020;384.

83. Malakootian M, Nasiri A, Asadipour A, Kargar E. Facile and green synthesis of ZnFe2O4@CMC as a new magnetic nanophotocatalyst for ciprofloxacin degradation from aqueous media. PROCESS SAFETY AND ENVIRONMENTAL PROTECTION. 2019;129:138–51.

84. Yan DY, Hu H, Gao NY, Ye JS, Ou HS. Fabrication of carbon nanotube functionalized MIL-101(Fe) for enhanced visible-light photocatalysis of ciprofloxacin in aqueous solution. APPLIED SURFACE SCIENCE. 2019;498.

85. Behera A, Kandi D, Mansingh S, Martha S, Parida K. Facile synthesis of ZnFe2O4@RGO nanocomposites towards photocatalytic ciprofloxacin degradation and H2 energy production. JOURNAL OF COLLOID AND INTERFACE SCIENCE. 2019;556:667–79.

86. Nasiri A, Tamaddon F, Mosslemin MH, Amiri Gharaghani MA, Asadipour A. Magnetic nano-biocomposite CuFe2 O4 @methylcellulose (MC) prepared as a new nano-photocatalyst for degradation of ciprofloxacin from aqueous solution. Environmental Health Engineering and Management. 2019;6(1):39–41.

87. Hassani A, Khataee A, Fathinia M, Karaca S. Photocatalytic ozonation of ciprofloxacin from aqueous solution using TiO2/MMT nanocomposite: Nonlinear modeling and optimization of the process via artificial neural network integrated genetic algorithm. PROCESS SAFETY AND ENVIRONMENTAL PROTECTION. 2018;116:365–76.

88. Khoshnamvand N, Kord Mostafapour F, Mohammadi A, Faraji M. Response surface methodology (RSM) modeling to improve removal of ciprofloxacin from aqueous solutions in photocatalytic process using copper oxide nanoparticles (CuO/UV). AMB Express. 2018;8(1).

89. Xing XB, Du ZX, Zhuang JC, Wang D. Removal of ciprofloxacin from water by nitrogen doped TiO2 immobilized on glass spheres: Rapid screening of degradation products. JOURNAL OF PHOTOCHEMISTRY AND PHOTOBIOLOGY A-CHEMISTRY. 2018;359:23–32.

90. Eskandari M, Goudarzi N, Moussavi SG. Application of low-voltage UVC light and synthetic ZnO nanoparticles to photocatalytic degradation of ciprofloxacin in aqueous sample solutions. WATER AND ENVIRONMENT JOURNAL. 2018;32(1):58–66.

91. Bekkali CE, Bouyarmane H, Karbane ME, Masse S, Saoiabi A, Coradin T, et al. Zinc oxide-hydroxyapatite nanocomposite photocatalysts for the degradation of ciprofloxacin and ofloxacin antibiotics. Colloids and Surfaces A: Physicochemical and Engineering Aspects. 2018;539:364–70.

92. Das S, Ghosh S, Misra AJ, Tamhankar AJ, Mishra A, Lundborg CS, et al. Sunlight Assisted Photocatalytic Degradation of Ciprofloxacin in Water Using Fe Doped ZnO Nanoparticles for Potential Public Health Applications. INTERNATIONAL JOURNAL OF ENVIRONMENTAL RESEARCH AND PUBLIC HEALTH. 2018;15(11).

93. Sayed M, Khan JA, Shah LA, Shah NS, Shah F, Khan HM, et al. Solar Light Responsive Poly(vinyl alcohol)-Assisted Hydrothermal Synthesis of Immobilized TiO2/Ti Film with the Addition of Peroxymonosulfate for Photocatalytic Degradation of Ciprofloxacin in Aqueous Media: A Mechanistic Approach. Journal of Physical Chemistry C. 2018;122(1):406–21.

94. Kumar A, Kumar A, Sharma G, Naushad M, Veses RC, Ghfar AA, et al. Solar-driven photodegradation of 17-β-estradiol and ciprofloxacin from waste water and CO2 conversion using sustainable coal-char/polymeric-g-C3N4/RGO metal-free nano-hybrids. New Journal of Chemistry. 2017;41(18):10208–24.

95. Bojer C, Schöbel J, Martin T, Ertl M, Schmalz H, Breu J. Clinical wastewater treatment: Photochemical removal of an anionic antibiotic (ciprofloxacin) by mesostructured high aspect ratio ZnO nanotubes. APPLIED CATALYSIS B-ENVIRONMENTAL. 2017;204:561–5.

96. Genç N. Improvement of the overall biodegradability of ciprofloxacin by pre-treatment with photocatalytic oxidation of wastewaters. Asian Journal of Water, Environment and Pollution. 2016;13(4):75–81.

97. Zhang XX, Li RP, Jia MK, Wang SL, Huang YP, Chen CC. Degradation of ciprofloxacin in aqueous bismuth oxybromide (BiOBr) suspensions under visible light irradiation: A direct hole oxidation

pathway. CHEMICAL ENGINEERING JOURNAL. 2015;274:290–7.

98. Lima M, Leblebici M, Dias M, Lopes J, Silva C, Silva A, et al. Continuous flow photo-Fenton treatment of ciprofloxacin in aqueous solutions using homogeneous and magnetically recoverable catalysts. ENVIRONMENTAL SCIENCE AND POLLUTION RESEARCH. 2014;21(19):11116–25.

99. Paul T, Dodd MC, Strathmann TJ. Photolytic and photocatalytic decomposition of aqueous ciprofloxacin: Transformation products and residual antibacterial activity. WATER RESEARCH. 2010;44(10):3121–32.

100. An T, Yang H, Li G, Song W, Cooper WJ, Nie X. Kinetics and mechanism of advanced oxidation processes (AOPs) in degradation of ciprofloxacin in water. Applied Catalysis B: Environmental. 2010;94(3-4):288–94.